Quartic coupling unification in the maximally symmetric 2HDM

Neda Darvishi[*] and Apostolos Pilaftsis[†]

Consortium for Fundamental Physics, School of Physics and Astronomy, University of Manchester, Manchester M13 9PL, United Kingdom

(Received 23 April 2019; published 10 June 2019)

We consider the maximally symmetric two-Higgs doublet model (MS-2HDM) in which the so-called Standard Model (SM) alignment can be naturally realized as a consequence of an accidental SO(5) symmetry in the Higgs sector. This symmetry is broken (i) explicitly by renormalization-group (RG) effects and (ii) softly by the bilinear scalar mass term m_{12}^2. We find that in the MS-2HDM all quartic couplings can unify at large RG scales $\mu_X \sim 10^{11}$–10^{20} GeV. In particular, we show that quartic coupling unification can take place in two different conformally invariant points, where all quartic couplings vanish. We perform a vacuum stability analysis of the model in order to ensure that the electroweak vacuum is sufficiently long-lived. The MS-2HDM is a minimal and very predictive extension of the SM governed by only three additional parameters: the unification scale μ_X, the charged Higgs mass $M_{h^\pm}$ (or m_{12}^2), and $\tan\beta$, which allow one to determine the entire Higgs sector of the model. In terms of these input parameters, we present illustrative predictions of misalignment for the SM-like Higgs-boson couplings to the $W^\pm$ and Z bosons and, for the first time to our knowledge, to the top and bottom quarks.

DOI: 10.1103/PhysRevD.99.115014

I. INTRODUCTION

Despite intense scrutiny, the Standard Model (SM) has proven to be very successful in describing the fundamental interactions of particle physics [1–3]. The discovery of the Higgs particle [4,5] at the CERN Large Hadron Collider (LHC) was one of the most important achievements toward a minimal ultraviolet (UV) completion of the SM [6,7]. In spite of its great success, the search for new physics beyond the SM still has strong theoretical and experimental motivations, and opens up new possibilities including the study of nonstandard scenarios with extended Higgs sectors. However, the latest LHC data dictate that the observed Higgs boson must interact with the electroweak (EW) gauge bosons (Z, $W^\pm$) with coupling strengths that are very close to their SM values [8,9]. This simple fact puts severe limits on possible scalar-sector extensions of the SM.

One class of minimal extensions of the SM is the two-Higgs doublet model (2HDM), where the SM scalar sector is extended by a second Higgs doublet [10,11]. This model can, in principle, account for a SM-like Higgs boson and contains additionally one charged and two neutral scalars whose observation could be within reach of the LHC [12,13].

In the 2HDM, one may have four different types of Yukawa interactions mediating no flavor changing neutral currents at the tree level [14–17]. More explicitly, in Type I (inert-type), all the fermions couple to the first doublet Φ_1 and none to the second doublet Φ_2. In Type II (MSSM-type), the down-type quarks and the charged leptons couple to Φ_1, and the up-type quarks couple to Φ_2. In Type III (flipped-model), the down-type quarks couple to Φ_1, and the up-type quarks and the charged leptons couple to Φ_2. In Type IV (lepton-specific model), all quarks couple to Φ_1, and the charged leptons couple to Φ_2. As mentioned above, in all these different settings of the 2HDM, the couplings of the SM-like Higgs boson to the electroweak gauge bosons (Z, $W^\pm$) must be very close to those predicted by the SM, so as to be in agreement with the current Higgs signals at the LHC. This is only possible within the so-called SM alignment limit of the 2HDM [18–25]. In particular, in the Type-II 2HDM, the couplings of the SM-like Higgs boson to vector bosons lie within 10% of the SM value at 95% C.L. [26–28].

In this paper, we consider the simplest realization of a Type-II 2HDM, the so-called maximally symmetric two-Higgs doublet model (MS-2HDM). In this model, the aforementioned SM alignment can emerge naturally as a consequence of an accidental SO(5) symmetry in the Higgs sector [22,29–31], without resorting to *ad hoc* arrangements among the parameters of the theory [21,32–36].

[*]neda.darvishi@manchester.ac.uk
[†]apostolos.pilaftsis@manchester.ac.uk

The SO(5) symmetry is broken explicitly by two sources: (i) by renormalization-group (RG) effects, and (ii) softly by the bilinear scalar mass term m_{12}^2. A remarkable feature of the MS-2HDM is that all quartic couplings can unify at very large scales $\mu_X \sim 10^{11}$–10^{20} GeV, for a wide range of $\tan\beta$ values and charged Higgs-boson masses. In particular, we find that quartic coupling unification can happen in two different conformally invariant points, where all quartic couplings vanish. The first conformal point is at a relatively low scale typically of order 10^{11} GeV, while the second one is at high scale close to the Planck scale $\sim 10^{19}$ GeV. Most remarkably, we find that the MS-2HDM becomes a very predictive extension of the SM which is governed by only three additional parameters: the quartic coupling unification scale μ_X, the charged Higgs mass $M_{h^\pm}$ (or m_{12}^2), and $\tan\beta$. These three parameters also suffice to determine the entire Higgs-mass spectrum of the model. By means of these input parameters, we are able to obtain definite predictions of misalignment for the SM-like Higgs-boson couplings to the $W^\pm$ and Z bosons and to the top and bottom quarks, which might be testable at future precision high-energy colliders.

The layout of the paper is as follows. After this introductory section, Sec. II briefly reviews the basic features of the 2HDM and discusses the conditions for achieving exact SM alignment. In Sec. III, we describe the MS-2HDM, thereby illuminating the origin of *natural* SM alignment. We also outline the breaking pattern of the SO(5) symmetry, which results from the soft-breaking mass m_{12}^2 and the RG effects, and discuss its implications for the Higgs-mass spectrum. In Sec. IV, we analyze in more detail the impact of RG effects up to two loops on all relevant quartic couplings by considering their running from the quartic coupling unification scale μ_X to the charged Higgs-boson mass. In particular, we show that the running quartic couplings can be unified at two different conformally invariant points. In the same section, we present illustrative predictions for the unification of all quartic couplings for typical values of $\tan\beta$ and charged Higgs-boson masses. Section V presents our misalignment predictions for Higgs-boson couplings to gauge bosons and top and bottom quarks. In Sec. VI, we analyze the EW vacuum lifetime of the MS-2HDM by considering the bounce solution to the Euclidean equation of motion for the classical potential, with a negative running quartic coupling λ_2. We estimate the EW vacuum lifetime τ which turns out to be adequately long, being many orders of magnitude larger than the age of the Universe (in the absence of Plank-scale suppressed operators [37,38]). Finally, Sec. VII contains our conclusions.

II. TYPE-II 2HDM AND SM ALIGNMENT

The Higgs sector of the 2HDM is described by two scalar SU(2) doublets,

$$\Phi_1 = \begin{pmatrix} \phi_1^+ \\ \phi_1^0 \end{pmatrix}, \qquad \Phi_2 = \begin{pmatrix} \phi_2^+ \\ \phi_2^0 \end{pmatrix}. \tag{2.1}$$

In terms of these doublets, the most general $\mathrm{SU}(2)_L \otimes \mathrm{U}(1)_Y$-invariant Higgs potential is given by

$$\begin{aligned} V = &-\mu_1^2(\Phi_1^\dagger\Phi_1) - \mu_2^2(\Phi_2^\dagger\Phi_2) - [m_{12}^2(\Phi_1^\dagger\Phi_2) + \text{H.c.}] \\ &+ \lambda_1(\Phi_1^\dagger\Phi_1)^2 + \lambda_2(\Phi_2^\dagger\Phi_2)^2 + \lambda_3(\Phi_1^\dagger\Phi_1)(\Phi_2^\dagger\Phi_2) \\ &+ \lambda_4(\Phi_1^\dagger\Phi_2)(\Phi_2^\dagger\Phi_1) + \Big[\frac{1}{2}\lambda_5(\Phi_1^\dagger\Phi_2)^2 \\ &+ \lambda_6(\Phi_1^\dagger\Phi_1)(\Phi_1^\dagger\Phi_2) + \lambda_7(\Phi_1^\dagger\Phi_2)(\Phi_2^\dagger\Phi_2) + \text{H.c.}\Big], \end{aligned} \tag{2.2}$$

where the mass term m_{12}^2 and quartic couplings λ_5, λ_6, and λ_7 are complex parameters. Instead, the remaining mass terms, μ_1^2 and μ_2^2, and the quartic couplings $\lambda_{1,2,3,4}$ are real. Of these 14 theoretical parameters, only 11 are physical, since three can be removed using a SU(2) reparametrization of the Higgs doublets Φ_1 and Φ_2 [34].

In the present article, we will restrict our attention to CP conservation and to CP-conserving vacua. In the Type-II 2HDM, both scalar doublets Φ_1 and Φ_2 receive nonzero vacuum expectation values (VEVs). Specifically, we have $\langle\phi_1^0\rangle = v_1/\sqrt{2}$ and $\langle\phi_2^0\rangle = v_2/\sqrt{2}$, where $v_{1,2}$ are nonzero and $v \equiv \sqrt{v_1^2 + v_2^2}$ is the VEV of the SM Higgs doublet. The minimization conditions resulting from the 2HDM potential in (2.2) give rise to the following relations:

$$\mu_1^2 = m_{12}^2 t_\beta - \frac{1}{2}v^2 c_\beta^2(2\lambda_1 + 3\lambda_6 t_\beta + \lambda_{345} t_\beta^2 + \lambda_7 t_\beta^3), \tag{2.3}$$

$$\mu_2^2 = m_{12}^2 t_\beta^{-1} - \frac{1}{2}v^2 s_\beta^2(2\lambda_1 + 3\lambda_6 t_\beta^{-1} + \lambda_{345} t_\beta^{-2} + \lambda_7 t_\beta^{-3}), \tag{2.4}$$

where $s_\beta \equiv \sin\beta$, $c_\beta \equiv \cos\beta$, $t_\beta \equiv \tan\beta = v_2/v_1$, and $\lambda_{345} \equiv \lambda_3 + \lambda_4 + \lambda_5$. Following the standard linear expansion of the two scalar doublets Φ_j (with $j = 1, 2$) about their VEVs, we may conveniently reexpress them as

$$\Phi_j = \begin{pmatrix} \phi_j^+ \\ \frac{1}{\sqrt{2}}(v_j + \phi_j + i\phi_j^0) \end{pmatrix}. \tag{2.5}$$

After spontaneous symmetry breaking (SSB), the standard EW gauge fields, the $W^\pm$ and Z bosons, acquire their masses from the three would-be Goldstone bosons $(G^\pm, G^0)$ [39]. As a consequence, the model has only five physical scalar states: two CP-even scalars (h,H), one CP-odd scalar (a), and two charged bosons $(h^\pm)$. The mixings in the CP-odd and charged scalar sectors are individually governed by the same angle β,

$$G^{\pm} = c_\beta \phi_1^{\pm} + s_\beta \phi_2^{\pm}, \qquad h^{\pm} = -s_\beta \phi_1^{\pm} + c_\beta \phi_2^{\pm},$$
$$G^0 = c_\beta \phi_1 + s_\beta \phi_2, \qquad a = -s_\beta \phi_1 + c_\beta \phi_2. \tag{2.6}$$

Correspondingly, the masses of the $h^{\pm}$ and a scalars are given by

$$M_{h^{\pm}}^2 = \frac{m_{12}^2}{s_\beta c_\beta} - \frac{v^2}{2}(\lambda_4 + \lambda_5) + \frac{v^2}{2 s_\beta c_\beta}(\lambda_6 c_\beta^2 + \lambda_7 s_\beta^2),$$
$$M_a^2 = M_{h^{\pm}}^2 + \frac{v^2}{2}(\lambda_4 - \lambda_5). \tag{2.7}$$

To obtain the masses of the two CP-even scalars, h and H, we need to diagonalize the two-by-two CP-even mass matrix M_S^2,

$$M_S^2 = \begin{pmatrix} A & C \\ C & B \end{pmatrix}, \tag{2.8}$$

which may explicitly be written down as

$$M_S^2 = M_a^2 \begin{pmatrix} s_\beta^2 & -s_\beta c_\beta \\ -s_\beta c_\beta & c_\beta^2 \end{pmatrix} + v^2 \begin{pmatrix} 2\lambda_1 c_\beta^2 + \lambda_5 s_\beta^2 + 2\lambda_6 s_\beta c_\beta & \lambda_{34} s_\beta c_\beta + \lambda_6 c_\beta^2 + \lambda_7 s_\beta^2 \\ \lambda_{34} s_\beta c_\beta + \lambda_6 c_\beta^2 + \lambda_7 s_\beta^2 & 2\lambda_2 s_\beta^2 + \lambda_5 c_\beta^2 + 2\lambda_7 s_\beta c_\beta \end{pmatrix},$$

with $\lambda_{34} \equiv \lambda_3 + \lambda_4$. The mixing angle α necessary for the diagonalization of M_S^2 may be determined by

$$\tan 2\alpha = \frac{2C}{A - B}. \tag{2.9}$$

The SM Higgs field may now be identified by the linear field combination,

$$H_{\rm SM} = \phi_1 \cos\beta + \phi_2 \sin\beta = H\cos(\beta - \alpha) + h \sin(\beta - \alpha). \tag{2.10}$$

In this way, one can obtain the SM-normalized couplings of the CP-even h and H scalars to the EW gauge bosons ($V = W^{\pm}, Z$) as follows:

$$g_{hVV} = \sin(\beta - \alpha), \qquad g_{HVV} = \cos(\beta - \alpha), \tag{2.11}$$

with $g_{H_{\rm SM}VV} = 1$ by definition. In a similar manner, we may derive the SM-normalized couplings of the CP-even and CP-odd scalars to up-type and down-type quarks. These couplings are exhibited in Table I.

From Table I, we observe that there are two ways to realize the SM alignment limit:

(i) SM-like h scenario: $M_h \approx 125$ GeV, $\sin(\beta - \alpha) = 1$ with $\beta - \alpha = \pi/2$.

(ii) SM-like H scenario: $M_H \approx 125$ GeV, $\cos(\beta - \alpha) = 1$ with $\beta = \alpha$.

In these limits, the CP-even $H(h)$ scalar couples to the EW gauge bosons with coupling strength exactly as that of the SM Higgs boson, while $h(H)$ does not couple to them at all [22]. In the above two scenarios, the SM-like Higgs boson is identified with the 125 GeV resonance observed at the LHC [6,7]. In the literature, the neutral Higgs partner (H) in the SM-like h scenario is usually termed the heavy Higgs boson. Instead, in the SM-like H scenario, the partner particle h can only have a mass smaller than ~125 GeV [23]. In this paper, we consider the alignment limit with $\beta = \alpha$, which falls in the category of the SM-like H scenario, but the CP-even scalar partner h can be either lighter or heavier than the observed scalar resonance at the LHC. In the alignment limit, the SM-like Higgs boson becomes aligned with one of the neutral eigenstates.

In the so-called Higgs basis [32], the CP-even mass matrix M_S^2 given in (2.8) takes on the form

$$\hat{M}_S^2 = \begin{pmatrix} c_\beta & s_\beta \\ -s_\beta & c_\beta \end{pmatrix} M_S^2 \begin{pmatrix} c_\beta & -s_\beta \\ s_\beta & c_\beta \end{pmatrix} = \begin{pmatrix} \hat{A} & \hat{C} \\ \hat{C} & \hat{B} \end{pmatrix}, \tag{2.12}$$

with

TABLE I. Tree-level couplings of a neutral scalar boson S (with $S = h, H, a$) to the $W^{\pm}$ and Z bosons and to quarks in the Type-II 2HDM.

S	g_{SVV} $(V = W^{\pm}, Z)$	g_{Suu}	g_{Sdd}
h	$\sin(\beta - \alpha)$	$\sin(\beta - \alpha) + \frac{1}{\tan\beta}\cos(\beta - \alpha)$	$\sin(\beta - \alpha) - \tan\beta \cos(\beta - \alpha)$
H	$\cos(\beta - \alpha)$	$\cos(\beta - \alpha) - \frac{1}{\tan\beta}\sin(\beta - \alpha)$	$\cos(\beta - \alpha) + \tan\beta \sin(\beta - \alpha)$
a	0	$-i\gamma_5 \cot\beta$	$-i\gamma_5 \tan\beta$

$$\hat{A} = 2v^2[c_\beta^4\lambda_1 + s_\beta^2 c_\beta^2\lambda_{345} + s_\beta^4\lambda_2 + 2s_\beta c_\beta(c_\beta^2\lambda_6 + s_\beta^2\lambda_7)],$$
$$\hat{B} = M_a^2 + \lambda_5 v^2 + 2v^2[s_\beta^2 c_\beta^2(\lambda_1 + \lambda_2 - \lambda_{345}) - s_\beta c_\beta(c_\beta^2 - s_\beta^2)(\lambda_6 - \lambda_7)],$$
$$\hat{C} = v^2[s_\beta^3 c_\beta(2\lambda_2 - \lambda_{345}) - c_\beta^3 s_\beta(2\lambda_1 - \lambda_{345}) + c_\beta^2(1 - 4s_\beta^2)\lambda_6 + s_\beta^2(4c_\beta^2 - 1)\lambda_7]. \quad (2.13)$$

The SM alignment limit, $\cos(\beta - \alpha) \to 1$, can be realized in two different ways: (i) $\hat{C} \to 0$ and (ii) $M_{h^\pm} \sim M_a \gg v$. The first realization (i) does not depend on the choice of the non-SM scalar masses, such as $M_{h^\pm}$ and M_a, whereas the second one (ii) is only possible in the well-known decoupling limit [32–34]. In the first case, SM alignment is obtained by setting $\hat{C} = 0$, which in turn implies the condition [22]

$$\lambda_7 t_\beta^4 - (2\lambda_2 - \lambda_{345})t_\beta^3 + 3(\lambda_6 - \lambda_7)t_\beta^2 + (2\lambda_1 - \lambda_{345})t_\beta - \lambda_6 = 0. \quad (2.14)$$

Barring fine-tuning among quartic couplings, (2.14) leads to the following constraints:

$$\lambda_1 = \lambda_2 = \frac{\lambda_{345}}{2}, \qquad \lambda_6 = \lambda_7 = 0, \quad (2.15)$$

which are independent of $\tan\beta$ and nonstandard scalar masses. In this case, the two CP-even Higgs masses in the alignment limit are given by

$$M_H^2 = 2v^2(\lambda_1 c_\beta^4 + \lambda_{345} s_\beta^2 c_\beta^2 + \lambda_2 s_\beta^4) \equiv 2\lambda_{\rm SM} v^2, \quad (2.16)$$

$$M_h^2 = M_a^2 + \lambda_5 v^2 + 2v^2 s_\beta^2 c_\beta^2(\lambda_1 + \lambda_2 - \lambda_{345}). \quad (2.17)$$

In the second realization (ii) mentioned above, we may simplify matters by expanding $M_{H,h}^2$ in powers of $v/M_a \ll 1$. In this way, we obtain [22]

$$M_H^2 \simeq 2\lambda_{\rm SM} v^2 - \frac{v^4 s_\beta^2 c_\beta^2}{M_a^2 + \lambda_5 v^2} \times [s_\beta^2(2\lambda_2 - \lambda_{345}) - c_\beta^2(2\lambda_1 - \lambda_{345})]^2, \quad (2.18)$$

$$M_h^2 \simeq M_a^2 + \lambda_5 v^2 \gg v^2. \quad (2.19)$$

Note that at large $\tan\beta$, the phenomenological properties of the H-boson resemble more and more those of the SM Higgs boson [20,21]. Since we are interested in analyzing the deviation of the H-boson couplings from their SM values, we follow an approximate approach inspired by the seesaw mechanism [40]. In particular, we may express all the H-boson couplings in terms of the light-to-heavy scalar-mixing parameter $\hat{C}/\hat{B}$. Thus, employing (2.9) for the hatted quantities and ignoring $\hat{A}$ next to $\hat{C}$, we may derive the approximate analytic expressions

$$g_{HVV} \simeq 1 - \frac{\hat{C}^2}{2\hat{B}^2}, \quad (2.20a)$$

$$g_{hVV} \simeq -\frac{\hat{C}}{\hat{B}} = \frac{v^2 s_\beta c_\beta}{M_a^2 + \lambda_5 v^2}[c_\beta^2(2\lambda_1 - \lambda_{345}) - s_\beta^2(2\lambda_2 - \lambda_{345})]. \quad (2.20b)$$

Given the tight experimental limits on the deviation of g_{HVV} from 1, one must have that the light-to-heavy scalar mixing parameter $\hat{C}/\hat{B} \ll 1$, which justifies our seesaw-inspired approximation. In fact, in the exact SM alignment limit, $\alpha \to \beta$, the mixing parameter $\hat{C}/\hat{B}$ vanishes identically.

In a similar fashion, we may derive approximate analytic expressions for the h- and H-boson couplings to up- and down-type quarks. To leading order in the light-to-heavy scalar mixing $\hat{C}/\hat{B}$, these are given by

$$g_{huu} \simeq -\frac{\hat{C}}{\hat{B}} + \frac{1}{\tan\beta}, \quad (2.21a)$$

$$g_{hdd} \simeq -\frac{\hat{C}}{\hat{B}} - \tan\beta, \quad (2.21b)$$

$$g_{Huu} \simeq 1 + \frac{1}{\tan\beta}\frac{\hat{C}}{\hat{B}}, \quad (2.21c)$$

$$g_{Hdd} \simeq 1 - \frac{\hat{C}}{\hat{B}}\tan\beta. \quad (2.21d)$$

In the SM alignment limit, we have $g_{Huu} \to 1$ and $g_{Hdd} \to 1$. Obviously, any deviation of the g_{Huu} and g_{Hdd} couplings from their SM values is controlled by $\tan\beta$ and $\hat{C}/\hat{B}$.

In the present study, our primary interest lies in natural realizations of SM alignment, for which neither a mass hierarchy $M_a \gg v$ nor a fine-tuning among the quartic couplings will be necessary. To this end, one is therefore compelled to identify possible maximal symmetries of the 2HDM potential that would impose the condition stated in (2.14). In the next section, we will show how SM alignment can be achieved naturally by virtue of an SO(5) symmetry imposed on the theory.

III. THE MAXIMALLY SYMMETRIC 2HDM

A convenient field basis to describe the 2HDM potential will be to make use of an eight-dimensional $\mathrm{SU}(2)_L$-covariant multiplet representation [41,42],

$$\mathbf{\Phi} = \begin{pmatrix} \Phi_1 \\ \Phi_2 \\ \tilde{\Phi}_1 \\ \tilde{\Phi}_2 \end{pmatrix}, \quad (3.1)$$

with $\tilde{\Phi}_{1,2} = i\sigma_2\Phi^*_{1,2}$. With the help of the multiplet $\mathbf{\Phi}$, a six-dimensional Lorentz vector $R^A = \Phi^\dagger\Sigma^A\Phi$ may be constructed, where $A = 0, 1, \ldots, 5$ and Σ^A are (8×8)-dimensional matrices whose precise analytic form is given in [29,41]. In this bilinear field-space formalism, R^A transforms under the *orthochronous* SO(1,5) symmetry group [22,29]. Since the $\mathrm{SU}(2)_L$ gauge-kinetic terms of the scalar doublets $\Phi_{1,2}$ must be canonical, the set of SO(1,5) rotations reduces to those of SO(5). So, in the absence of the hypercharge gauge coupling g' and fermion Yukawa couplings, the maximal symmetry group of the 2HDM is SO(5). As a consequence, the 2HDM potential has a total of 13 accidental symmetries [41], of which 6 preserve $\mathrm{U}(1)_Y$ [43–45] and 7 are custodially symmetric [29]. Given the isomorphism of the Lie algebras, $\mathrm{SO}(5) \sim \mathrm{Sp}(4)$, the maximal symmetry group of the 2HDM in the original $\mathbf{\Phi}$-field space is $G^{\mathbf{\Phi}}_{\mathrm{2HDM}} = [\mathrm{Sp}(4)/\mathrm{Z}_2]\times \mathrm{SU}(2)_L$ [29]. In the Type-II 2HDM, the maximal symmetry group SO(5) is the simplest of the three possible symmetries that can realize natural SM alignment. The other two are in bilinear [original] field space [22]: (i) $\mathrm{O}(3)\otimes \mathrm{O}(2)[\mathrm{SU}(2)_{\mathrm{HF}}]$, and (ii) $\mathrm{Z}_2 \otimes [\mathrm{O}(2)]^2[\mathrm{SO}(2)_{\mathrm{HF}}\times CP]$. In what follows, we focus on the simplest realization of SM alignment, which is called the MS-2HDM.

In the MS-2HDM, the SO(5) symmetry puts severe restrictions on the allowed form of the kinematic parameters of the 2HDM potential in (2.2),

$$\mu_1^2 = \mu_2^2, \qquad m_{12}^2 = 0,$$
$$\lambda_2 = \lambda_1, \qquad \lambda_3 = 2\lambda_1, \qquad \lambda_4 = \mathrm{Re}(\lambda_5) = \lambda_6 = \lambda_7 = 0. \tag{3.2}$$

Evidently, the MS-2HDM potential obeys naturally the alignment constraints given in (2.15). As a consequence, the scalar potential takes on a very simple form,

$$V = -\mu^2(|\Phi_1|^2 + |\Phi_2|^2) + \lambda(|\Phi_1|^2 + |\Phi_2|^2)^2 + \Delta V, \tag{3.3}$$

where

$$\Delta V = \sum_{i,j=1,2}^{i\neq j} m_{ij}^2(\Phi_i^\dagger\Phi_j) \tag{3.4}$$

are soft SO(5)-breaking mass terms, which are introduced here for phenomenological reasons as we will explain below.

After EW symmetry breaking, the following breaking pattern emerges:

$$\mathrm{SO}(5) \xrightarrow{\langle\Phi_{1,2}\rangle\neq 0} \mathrm{SO}(4). \tag{3.5}$$

If $\Delta V = 0$, the CP-even scalar H receives a nonzero squared mass $M_H^2 = 2\lambda_2 v^2$, while the other scalars, h, a, and $h^\pm$, are all massless. These are massless pseudo-Goldstone bosons that have sizable couplings to the SM gauge bosons. Accordingly, several experimentally excluded decay channels would open, e.g., $Z \to ha$ and $W^\pm \to h^\pm h$ [46]. If the SO(5) symmetry is realized at some high energy scale μ_X (much above the EW scale), then due to RG effects the following breaking pattern may take place [22]:

$$\begin{aligned}\mathrm{SO}(5)\otimes\mathrm{SU}(2)_L &\xrightarrow{g'\neq 0} \mathrm{O}(3)\otimes\mathrm{O}(2)\otimes\mathrm{SU}(2)_L\\ &\sim \mathrm{O}(3)\otimes\mathrm{U}(1)_Y\otimes\mathrm{SU}(2)_L\\ &\xrightarrow{\text{Yukawa}} \mathrm{O}(2)\otimes\mathrm{U}(1)_Y\otimes\mathrm{SU}(2)_L\\ &\sim \mathrm{U}(1)_{\mathrm{PQ}}\otimes\mathrm{U}(1)_Y\otimes\mathrm{SU}(2)_L\\ &\xrightarrow{\langle\Phi_{1,2}\rangle\neq 0} \mathrm{U}(1)_{\mathrm{em}}.\end{aligned} \tag{3.6}$$

Note that the RG effect of the gauge coupling g' only lifts the charged Higgs mass $M_{h^\pm}$, while the corresponding effect of the Yukawa couplings (particularly that of the top quark y_t) renders the other CP-even pseudo-Goldstone boson h massive. Instead, the CP-odd scalar a remains massless and can be identified with a Peccei-Quinn (PQ) axion after the SSB of a global $\mathrm{U}(1)_{\mathrm{PQ}}$ symmetry [47–49]. Since weak-scale PQ axions have been ruled out by experiment, we have allowed for the SO(5) symmetry of the MS-2HDM potential in (3.3) to be broken by the soft SO(5)-breaking mass terms in (3.4). Hence, without loss of generality, we may consider that only the soft SO(5)-breaking parameter $\mathrm{Re}(m_{12}^2)$ is nonzero. With this minimal addition to the MS-2HDM potential, the scalar-boson masses are given, to a very good approximation, by

$$M_H^2 = 2\lambda_2 v^2, \qquad M_h^2 = M_a^2 = M_{h^\pm}^2 = \frac{\mathrm{Re}(m_{12}^2)}{s_\beta c_\beta}. \tag{3.7}$$

Hence, all pseudo-Goldstone bosons, h, a, and $h^\pm$, become massive and almost degenerate in mass. As we will see in the next section, this degeneracy is very stable against RG effects even up to two-loop order.

In our study, we will consider the charged Higgs boson mass $M_{h^\pm}$ as an input parameter above the 500 GeV range, in agreement with B-meson constraints [50]. It will also be our threshold above which all parameters run with 2HDM renormalization group equations (RGEs). Moreover, we implement the matching conditions with two-loop RG effects of the SM at given $M_{h^\pm}$ threshold scales. We also employ two-loop 2HDM RGEs to find the running of the gauge, Yukawa, and quartic couplings at RG scales larger than $M_{h^\pm}$. For reviews on one-, two-, and three-loop RGEs in the 2HDM, see [22,51–54]. The SM and the 2HDM RGEs have been computed using the public *Mathematica* package SARAH [55], which has been appropriately adapted for the MS-2HDM.

TABLE II. SM couplings evaluated at the two-loop level in the $\overline{\rm MS}$ scheme at various threshold scales $\mu_{\rm thr}$, i.e., for $\mu_{\rm thr} = M_t$ and $\mu_{\rm thr} = M_{h^\pm} = 500$ GeV, 1 TeV, 10 TeV, and 100 TeV.

$\mu_{\rm thr}$ [GeV]	g_1	g_2	g_3	$\lambda_{\rm SM}$	y_t	y_b	y_τ
M_t	0.3583	0.6779	1.1666	0.1292	0.9401	0.0157	0.010 00
500	0.3605	0.6423	1.0910	0.1102	0.8807	0.0146	0.010 08
10^3	0.3619	0.6388	1.0523	0.0997	0.8521	0.0140	0.010 12
10^4	0.3668	0.6274	0.9484	0.0719	0.7746	0.0123	0.010 22
10^5	0.3718	0.6164	0.8704	0.0518	0.7154	0.0111	0.010 26

IV. QUARTIC COUPLING UNIFICATION

As we saw in the previous section, the SO(5) symmetry of the MS-2HDM potential is broken explicitly by RG effects and soft-mass terms. In this section, we will consider a unified theoretical framework in which the SO(5) symmetry is realized at some high-energy scale μ_X, where all the conditions in (3.2) are met. Of particular interest is the potential existence of conformally invariant unification points at which all quartic couplings of the MS-2HDM potential vanish simultaneously.

To address the above issue of quartic coupling unification, we employ two-loop RGEs for the MS-2HDM from the unification scale μ_X to the charged Higgs-boson mass $M_{h^\pm} \ll \mu_X$. Below this threshold scale $\mu_{\rm thr} = M_{h^\pm}$, the SM is a good effective field theory, so we use the two-loop SM RGEs given in [56] to match the relevant MS-2HDM couplings to the corresponding SM quartic coupling $\lambda_{\rm SM}$, the Yukawa couplings, and the $\mathrm{SU}(2)_L$ and $\mathrm{U}(1)_Y$ gauge couplings g_2 and g' (with $g_1 = \sqrt{5/3}g'$). In order to obtain illustrative predictions, we have chosen our threshold scales to be at $\mu_{\rm thr} = M_{h^\pm} = 500$ GeV, 1 TeV, 10 TeV, and 100 TeV.

The theoretical SM parameters are determined in terms of precision observables, such as the Z-boson mass (M_Z), the $W^\pm$-boson mass (M_W), the Fermi constant G_μ, the strong coupling $\alpha_3(M_Z)$, the top-quark mass (M_t), and the Higgs boson mass ($M_{H_{\rm SM}}$). In detail, the following SM values will be adopted [57]:

$$\begin{aligned} M_W &= 80.384 \pm 0.014\ \text{GeV}, \\ M_Z &= 91.1876 \pm 0.0021\ \text{GeV}, \\ M_{H_{\rm SM}} &= 125.15 \pm 0.24\ \text{GeV}, \\ M_t &= 173.34 \pm 0.76 \pm 0.3\ \text{GeV}, \\ v &= (\sqrt{2}G)^{-1/2} = 246.21971 \pm 0.00006\ \text{GeV}, \\ \alpha_3(M_Z) &= 0.1184 \pm 0.0007. \end{aligned} \tag{4.1}$$

The values of the two-loop SM couplings at different threshold scales, $\mu_{\rm thr} = M_t$, $M_{h^\pm}$, are given in Table II.

The matching conditions for the Yukawa couplings at the threshold scale $\mu_{\rm thr} = M_{h^\pm}$ read

$$h_t^{\text{MS-2HDM}} = \frac{y_t}{s_\beta}, \quad h_b^{\text{MS-2HDM}} = \frac{y_b}{c_\beta}, \quad h_\tau^{\text{MS-2HDM}} = \frac{y_\tau}{c_\beta}. \tag{4.2}$$

Note that for RG scales $\mu > \mu_{\rm thr} = M_{h^\pm}$, the evolution of the Yukawa couplings h_t, h_b, and h_τ is governed by two-loop 2HDM RGEs.

Figures 1 and 2 display the RG evolution of all relevant couplings of the SM and the MS-2HDM, for $\tan\beta = 50$ and $m_{12}^2 \approx 70^2$ GeV^2 ($M_{h^\pm} = 500$ GeV). The vertical dashed line indicates the threshold scale $\mu_{\rm thr} = M_{h^\pm} = 500$ GeV. At this RG scale, we observe significant discontinuities in the running of Yukawa couplings y_b and y_τ due to the matching conditions in (4.2).

As can be seen from Fig. 1, the quartic coupling λ_2, which determines the SM-like Higgs-boson mass M_H, decreases at high RG scales due to the running of the top-Yukawa coupling h_t and turns negative just above the quartic coupling unification scale $\mu_X \sim 10^{11}$ GeV, at which all quartic couplings vanish. Thus, for energy scales above the RG scale μ_X, we envisage that the MS-2HDM will need to be embedded into another UV-complete theory. Nevertheless, according to our estimates in Sec. VI, we have checked that the resulting MS-2HDM potential leads to a metastable but sufficiently long-lived EW vacuum,

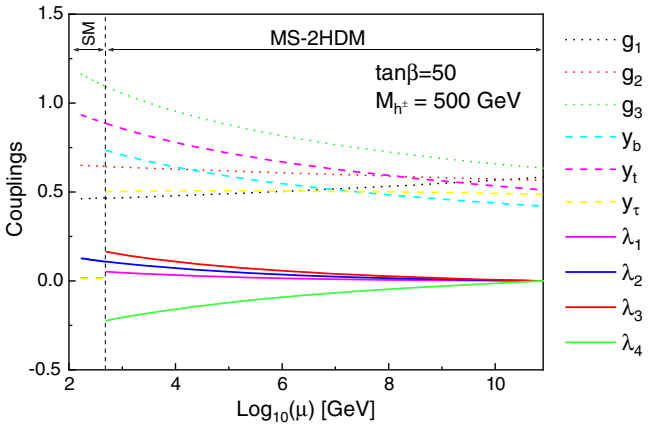

FIG. 1. The RG evolution of the quartic couplings $\lambda_{1,2,3,4}$ and the gauge and Yukawa couplings from the threshold scale $M_{h^\pm} = 500$ GeV up to their first quartic coupling unification scale $\mu_X^{(1)} = 10^{11}$ GeV for $\tan\beta = 50$.

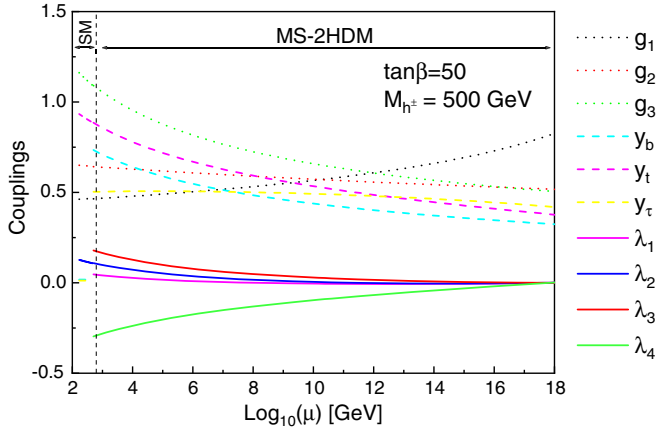

FIG. 2. The same as in Fig. 1, where the RG evolution extended up to the second quartic coupling unification point $\mu_X^{(2)} = 10^{18}$ GeV is shown.

whose lifetime is many orders of magnitude larger than the age of our Universe. In this respect, we regard the usual constraints derived from convexity conditions on 2HDM potentials [58] to be over-restrictive and unnecessary in our theoretical framework.

Of equal importance is a second conformally invariant unification point $\mu_X^{(2)}$ at energy scales close to the reduced Planck mass of order 10^{18} GeV, as shown in Fig. 2. In this case, the key quartic coupling λ_2 increases and becomes positive again. Hence, in this second class of settings, any embedding of the MS-2HDM into a UV-complete theory must have to take quantum gravity into account as well.

In Fig. 3, we give numerical estimates of the mass spectrum of the MS-2HDM, for $\tan\beta = 50$ and $m_{12}^2 \approx 70^2$ GeV^2 ($M_{h^\pm} = 500$ GeV). We find that all heavy Higgs bosons, h, a, and $h^\pm$, are approximately degenerate in mass, almost independently of the quartic coupling unification scale μ_X. In fact, to leading order, all masses are determined by the soft mass term m_{12}^2 in (3.7). The curve corresponding to the SM-like Higgs-boson mass M_H is mainly tracking $\lambda_2(\mu)$, which has two roots, one at RG scales around $\mu_X^{(1)} \sim 10^{11}$ GeV and another one at $\mu_X^{(2)} \sim 10^{18}$ GeV. The latter is the largest possible UV scale of the MS-2HDM.

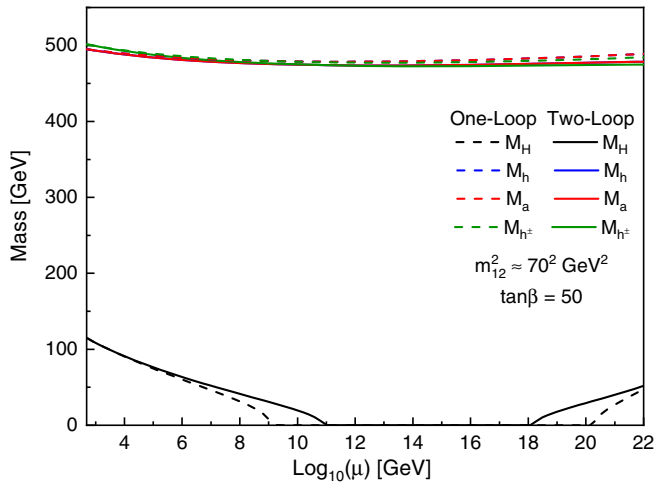

FIG. 3. The scalar mass spectrum of the MS-2HDM with $m_{12}^2 \approx 70^2$ GeV^2 and $\tan\beta = 50$. The dashed and the solid curves show the one-loop and the two-loop RGEs of the scalar masses, respectively.

Figure 4 shows all conformally invariant quartic coupling unification points in the $(\tan\beta, \log_{10}\mu)$ plane, by considering different values of threshold scales $\mu_{\rm thr}$, i.e., for $\mu_{\rm thr} = M_{h^\pm} = 500$ GeV, 1 TeV, 10 TeV, and 100 TeV. The lower curves (dashed curves) correspond to sets of low-scale quartic coupling unification points, while the upper curves (solid curves) give the corresponding sets of high-scale unification points. From Fig. 4, we may also observe the domains in which the λ_2 coupling becomes negative. These are given by the vertical μ-intervals bounded by the lower and the upper curves, for a given choice of $M_{h^\pm}$ and $\tan\beta$. Evidently, as the threshold scale $\mu_{\rm thr} = M_{h^\pm}$ increases, the size of the negative λ_2 domain increases and becomes more pronounced for smaller values of $\tan\beta$.

Before concluding this section, it is important to stress that the MS-2HDM requires only three additional input parameters: (i) the soft SO(5)-breaking mass parameter m_{12}^2 (or $M_{h^\pm}$), (ii) the ratio of VEVs $\tan\beta$, and (iii) the conformally invariant quartic coupling unification scale μ_X which can only assume two discrete values: $\mu_X^{(1)}$ and $\mu_X^{(2)}$. Once the values of these three theoretical parameters are given, the entire Higgs sector of the model can be determined. In the next section, we will give typical predictions in terms of these three input parameters.

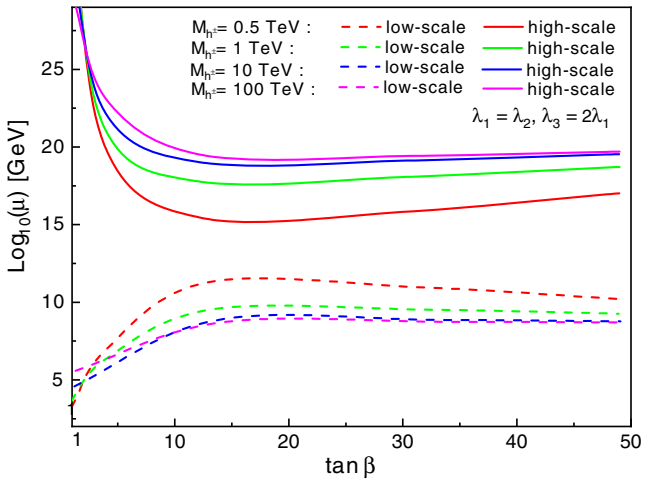

FIG. 4. Sets of quartic coupling unification points in the $(\tan\beta, \log_{10}\mu)$ plane, for charged Higgs-boson masses $M_{h^\pm} = 500$ GeV, 1 TeV, 10 TeV, and 100 TeV. The dashed and solid curves show the sets of low-scale and high-scale quartic coupling unification points, $\mu_X^{(1)}$ and $\mu_X^{(2)}$, respectively.

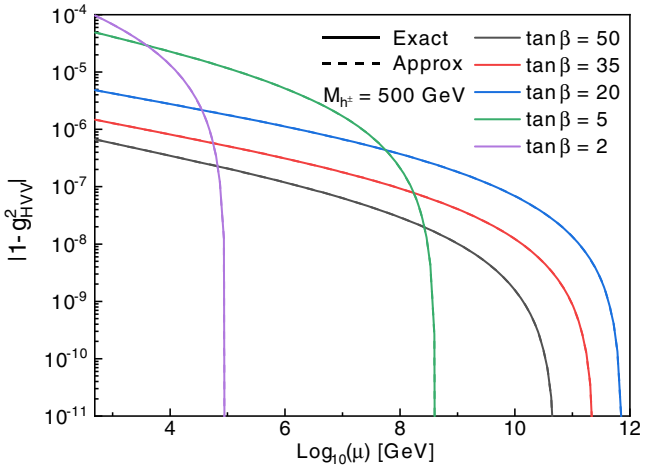

FIG. 5. Numerical estimates of the misalignment parameter $|1-g^2_{HVV}|$ pertinent to the HVV coupling (with $V=W^\pm,Z$) as functions of the RG scale μ, for a low-scale quartic coupling unification scenario, assuming $M_{h^\pm}=500$ GeV and $\tan\beta=2$, 5, 20, 35, and 50.

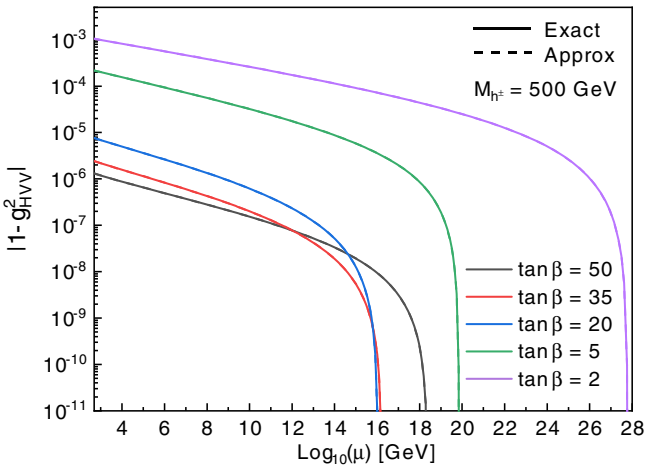

FIG. 6. The same as in Fig. 5, but for a high-scale quartic coupling unification scenario.

V. MISALIGNMENT PREDICTIONS FOR HIGGS BOSON COUPLINGS

In this section, we present numerical estimates of the predicted deviations of the SM-like Higgs-boson couplings HVV (with $V=W^\pm,Z$), $Ht\bar{t}$, and $Hb\bar{b}$, from their respective SM values. As was discussed in Sec. II, these deviations are controlled by the light-to-heavy scalar mixing parameter $\hat{C}/\hat{B}$. At the quartic coupling unification scale μ_X, the SO(5) symmetry of the MS-2HDM is fully restored and this mixing parameter vanishes. However, as we saw in Sec. III, RG effects induced by the $\mathrm{U}(1)_Y$ gauge coupling and the Yukawa couplings of the third generation of fermions break sizably the SO(5) symmetry, giving rise to a calculable nonzero value for $\hat{C}/\hat{B}$ and so to misalignment predictions for *all* H-boson couplings to SM particles.

In Figs. 5 and 6, we exhibit the dependence of the physical misalignment parameter $|1-g^2_{HVV}|$ (with $g_{H_{\rm SM}VV}=1$) as functions of the RG scale μ, for typical values of $\tan\beta$, such as $\tan\beta=2$, 5, 20, 35, and 50. As expected, we observe that the normalized coupling g_{HVV} approaches the SM value $g_{H_{\rm SM}VV}=1$ at the lower- and higher-scale quartic coupling unification points, $\mu_X^{(1)}$ and $\mu_X^{(2)}$, as shown in Figs. 5 and 6, respectively. We use dashed lines to display our predictions to leading order in $\hat{C}/\hat{B}$ expansion, while solid lines stand for the exact all-orders result. Since there is a small deviation (below the per-mile level) of g_{HVV} from the SM value, the approximate and exact predicted values are almost overlapping. Note that the misalignment reaches its maximum value for low values of $\tan\beta$ and for the higher quartic coupling unification points.

By analogy, Figs. 7 and 8 display misalignment predictions for the H-boson couplings to top and bottom quarks, for $\tan\beta=2$, 5, 20, 35, and 50 and for lower- and higher-scale quartic coupling unification points, respectively. As before, the deviation of the normalized couplings g_{Htt} and g_{Hbb} from their SM values are larger for low values

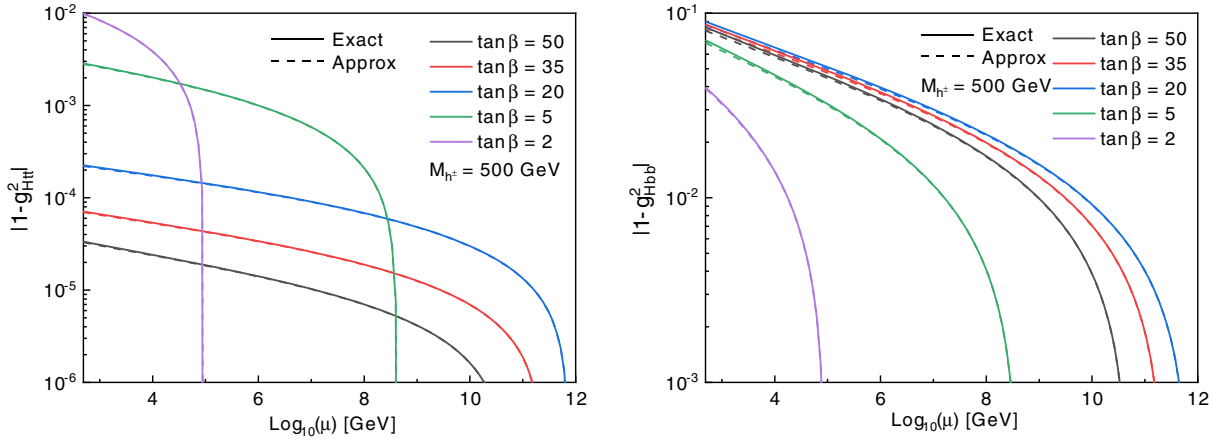

FIG. 7. The misalignment parameters $|1-g^2_{Htt}|$ (left panel) and $|1-g^2_{Hbb}|$ (right panel) versus the RG scale μ for a low-scale quartic coupling unification scenario, assuming $M_{h^\pm}=500$ GeV and $\tan\beta=2$, 5, 20, 35, and 50.

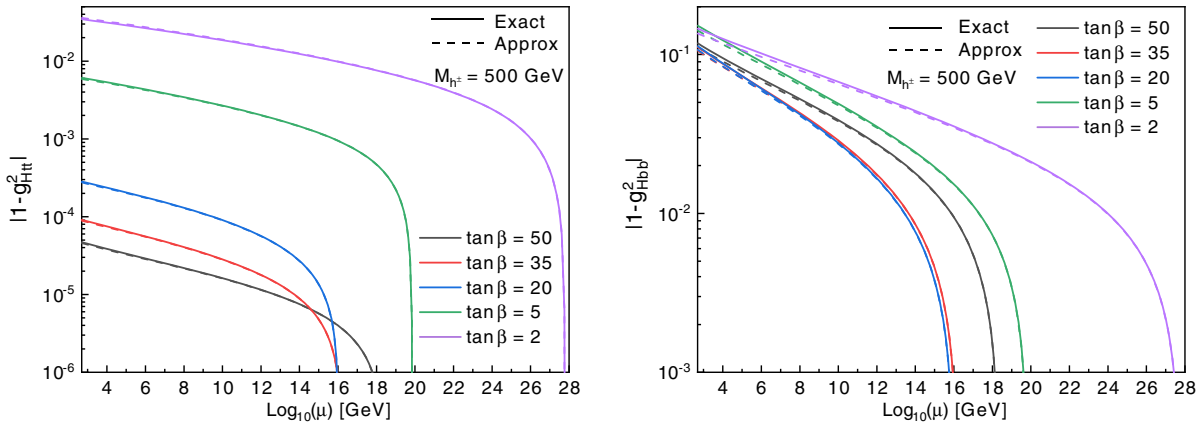

FIG. 8. The same as in Fig. 7, but for a high-scale quartic coupling unification scenario.

of $\tan\beta$, e.g., $\tan\beta = 2$, and for higher quartic coupling unification points $\mu_X^{(2)}$. This effect is more pronounced for g_{Hbb}, as the degree of misalignment might be even larger than 10%. In this case, a comparison between solid and dashed lines demonstrates the goodness of our seesaw-inspired approximation in terms of $\hat{C}/\hat{B}$.

Finally, we confront our misalignment predictions for the SM-like Higgs boson couplings, g_{HZZ}, g_{Htt}, and g_{Hbb} with existing experimental data from ATLAS and CMS, including their statistical and systematic uncertainties [59]. All these results are presented in Table III for $M_{h^\pm} = 500$ GeV. The observed results for g_{HZZ} and g_{Htt} are in excellent agreement with the SM and the MS-2HDM. Instead, the LHC data for g_{Hbb} can be fitted to the SM at the 3σ level. The latter reduces only to 2σ in the MS-2HDM, for $\tan\beta = 2$ assuming a high-scale quartic coupling unification scenario. Future precision collider experiments will be able to probe such a scenario.

VI. LIFETIME OF THE METASTABLE ELECTROWEAK VACUUM

According to our discussion in Sec. IV, we have seen that the MS-2HDM has two conformally invariant quartic coupling unification points $\mu_X^{(1,2)}$ for a given choice of the charged Higgs-boson mass $M_{h^\pm}$ and $\tan\beta$. Typically, the first point is at $\mu_X^{(1)} \sim 10^{11}$ GeV and the second one at $\mu_X^{(2)} \sim 10^{18}$ GeV. Between these two RG scales, i.e., for $\mu_X^{(1)} < \mu < \mu_X^{(2)}$, the running quartic coupling $\lambda_2(\mu)$ turns negative, which gives rise to a deeper minimum in the effective MS-2HDM potential. This new minimum will then be the *true vacuum* of the MS-2HDM. In this case, the EW vacuum that we currently live in becomes metastable and is usually called the *false vacuum*. For the high-scale quartic coupling unification scenario, this vacuum instability might be a problem, unless the lifetime of the EW vacuum is much larger than the age of the Universe.

In a general 2HDM, there are three different types of ground states [10,60,61]: (i) an EW-breaking vacuum that preserves CP and charge (normal minimum); (ii) an EW-breaking vacuum that breaks CP spontaneously but keeps charge conserved; and (iii) a charge-violating ground state, where one of the upper components $\phi^+_{1,2}$ of the scalar doublets $\Phi_{1,2}$ acquires a nonzero VEV. The existence of various minima in the potential may result in tunneling between different vacua. However, it is has been known for some time [62–64] that if the effective 2HDM potential has at least one CP- and charge-preserving local minimum, then any other possible charged-violating minimum cannot be deeper than this and so tunneling into such a local minimum will not be energetically favored. Hence, our

TABLE III. Predicted values of the SM-like Higgs boson couplings to the Z boson and to top and bottom quarks in the MS-2HDM for both scenarios with low- and high-scale quartic coupling unification, assuming $M_{h^\pm} = 500$ GeV. The corresponding central values for these couplings from ATLAS and CMS are also given, including their uncertainties [59].

Couplings	ATLAS	CMS	$\tan\beta = 2$	$\tan\beta = 5$	$\tan\beta = 20$	$\tan\beta = 35$	$\tan\beta = 50$
$\lvert g^{\text{low-scale}}_{HZZ}\rvert$	[0.86, 1.00]	[0.90, 1.00]	0.9999	0.9999	0.9999	0.9999	0.9999
$\lvert g^{\text{high-scale}}_{HZZ}\rvert$			0.9981	0.9998	0.9999	0.9999	0.9999
$\lvert g^{\text{low-scale}}_{Htt}\rvert$	$1.31^{+0.35}_{-0.33}$	$1.45^{+0.42}_{-0.32}$	1.0049	1.0014	1.0001	1.0000	1.0000
$\lvert g^{\text{high-scale}}_{Htt}\rvert$			1.0987	1.0179	1.0003	1.0001	1.0001
$\lvert g^{\text{low-scale}}_{Hbb}\rvert$	$0.49^{+0.26}_{-0.19}$	$0.57^{+0.16}_{-0.16}$	0.9803	0.9649	0.9560	0.9574	0.9590
$\lvert g^{\text{high-scale}}_{Hbb}\rvert$			0.8810	0.9264	0.9449	0.9456	0.9427

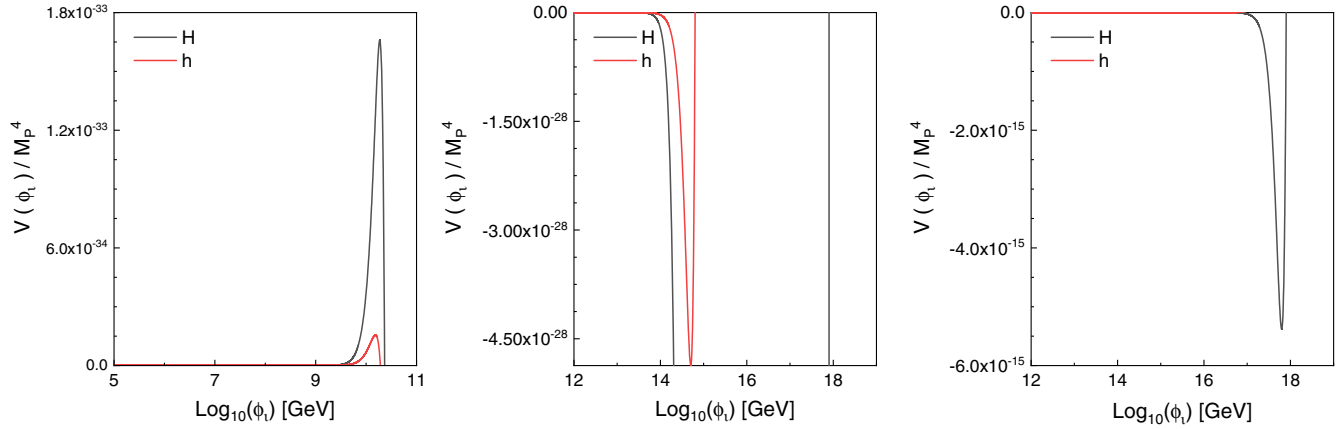

FIG. 9. The profile of the effective potential along the H- and h-field directions, with $\tan\beta = 50$ and $M_h^{\pm} = 500$ GeV. The potential along $H(h)$ is getting negative at scales around $\sim 10^{11}$ GeV and reaches a new minimum at roughly $\sim 10^{18}$ GeV ($\sim 10^{15}$ GeV).

false neutral EW vacuum can only tunnel to another neutral vacuum, and our findings are consistent with this observation in the MS-2HDM.

The probability rate P for quantum tunneling through a barrier is exponentially suppressed, and it may be estimated by

$$P \sim e^{-\Delta S_E}, \tag{6.1}$$

where ΔS_E is the Euclidean action evaluated at the $\mathbb{O}(4)$-symmetric bounce solution [66]. The action ΔS_E interpolates between the new phase at high field values and the EW phase. As we will see below, ΔS_E is the Euclidean action of the corresponding bounce minus the action of the false vacuum configuration [65]. To determine the lifetime of the false vacuum, we have to look for the so-called bounce solutions that satisfy the equations of motion,

$$\frac{d^2\phi_i}{dr^2} + \frac{3}{r}\frac{d\phi_i}{dr} = \frac{\partial V(\phi)}{\partial \phi_i}, \tag{6.2}$$

where the index $i = 1, 2, \ldots, 5$ labels all scalar fields $\phi_i = (h, H, a, h^+, h^-)$ and $\phi \equiv \{\phi_i\}$. Note that the fields ϕ_i depend only on the Euclidean radial coordinate $r = (t_E^2 + \mathbf{x}^2)^{1/2}$, as a consequence of the $\mathbb{O}(4)$ symmetry of the problem. The boundary conditions of the equations of motion are

$$\left.\frac{d\phi_i}{dr}\right|_{r=0} = 0, \qquad \lim_{r\to\infty}(\phi_i) = \phi_i^{\rm fv}, \tag{6.3}$$

where $\phi_i^{\rm fv}$ are the values of the fields ϕ_i at the false vacuum. More explicitly, the action $\Delta S_{E,i}$ along a ϕ_i direction is given by [66]

$$\Delta S_{E,i} \equiv S[\phi_i^{\rm b}] - S[\phi_i^{\rm fv}] = -\frac{\pi^2}{2}\int_0^\infty dr r^3 \frac{\partial V(\phi^{\rm b})}{\partial \phi_i^{\rm b}}\phi_i^{\rm b}. \tag{6.4}$$

Here, $\phi^{\rm b} \equiv \{\phi_i^{\rm b}\}$ denotes collectively the bounce solutions satisfying the boundary conditions stated in (6.3). For our MS-2HDM scenario, we have five second-order differential equations to determine the bounce configurations, where $r = 0$ is the center of the bounce which asymptotically approaches the false vacuum $\phi^{\rm fv} \equiv \{\phi_i^{\rm fv}\}$ as $r \to \infty$.

As the second deeper minimum of the potential occurs at field values $\phi_i \gg v$, where typically $\phi_i \gtrsim 10^{10}$ GeV, it will be a good approximation if we only keep its quartic terms. Therefore, the EW vacuum lifetime is computed by considering only the scale-invariant part of the effective potential:

$$V(\mu \gg v) \approx \frac{1}{4}[\lambda_1 h^4 + \lambda_2 H^4 + 2(\lambda_3 + \lambda_4)h^2H^2], \tag{6.5}$$

where the running quartic coupling λ_2 is negative. This analytic approximation leads to the following Euclidean action for the Fubini instanton [67]:

$$\Delta S_{E,i} \simeq -\frac{8\pi^2}{3|\lambda_i|}, \tag{6.6}$$

where $i = 1, 2$. Knowing $\Delta S_{E,i}$, an approximate formula for the EW vacuum lifetime τ in units of the age of the Universe ($T_U \sim 13.7 \times 10^9$ yr) for the individual quantum tunnelings from the EW vacuum to a deeper minimum in the ϕ_i direction ($\phi_1 = h$ and $\phi_2 = H$) may be derived,

$$\tau_i = \frac{e^{\Delta S_{E,i}}}{\phi_i(0)^4 T_U^4}. \tag{6.7}$$

Figure 9 gives the profile of the MS-2HDM potential along the H- (black curves) and h- (red curves) field directions. By considering the running quartic couplings, the instability shown in Fig. 9 occurs when λ_2 crosses zero and becomes negative after the first unification point $\mu_X^{(1)}$. Note that the scalar potential along the field direction of the SM-like Higgs boson H has a higher maximum and a deeper minimum compared to those found along the h direction.

TABLE IV. Numerical values for the center of the bounce solution divided by the Plank mass M_P for neutral CP-even Higgs bosons h and H, including their respective contributions to the EW vacuum lifetime τ in units of the age of the Universe T_U. The values of the quartic couplings $\lambda_{1,2,3,4}$ at the center of the bounce solution are also given.

	$\phi_i(0)/M_P$	λ_1	λ_2	λ_3	λ_4	τ_i/T_U
H	1.73×10^{-5}	4.2×10^{-4}	-2.05×10^{-3}	-9.86×10^{-3}	2.818×10^{-2}	$\sim 10^{5400}$
h	5.06×10^{-7}	-1.6×10^{-4}	-1.11×10^{-3}	-4.42×10^{-3}	1.162×10^{-2}	$\sim 10^{114180}$

Table IV presents the results of our analysis, which gives the center of the bounce solution $\phi_i^{\rm b}(0)$ for the neutral CP-even Higgs bosons H and h, divided by the Plank mass $M_P \approx 1.9 \times 10^{19}$ GeV. The same table includes numerical estimates of the EW vacuum lifetimes τ_h and τ_H, as well as the values of the effective quartic couplings $\lambda_{1,2,3,4}$ at the center of the bounce solution.

We find that the EW vacuum lifetime τ is many orders of magnitude larger than the age of the Universe, and even much larger than the SM EW vacuum lifetime $\tau_{\rm SM} \sim 10^{640} T_U$ in the flat space (in the absence of Plank-scale suppressed operators [37,38]). Therefore, we safely conclude that our Universe is adequately stable and so our high-scale quartic coupling unification scenario is phenomenologically viable.

VII. CONCLUSIONS

We have considered one of the simplest realizations of a Type-II 2HDM, the so-called maximally symmetric two-Higgs doublet model. The scalar potential of this model is determined by a single quartic coupling and a single mass parameter. This minimal form of the potential can be reinforced by an accidental SO(5) symmetry in the bilinear field space, which is isomorphic to $\mathrm{Sp}(4)/Z_2$ in the field basis $\mathbf{\Phi}$ given in (3.1). The MS-2HDM can naturally realize the so-called SM alignment limit, in which all SM-like Higgs boson couplings to $W^\pm$ and Z bosons and to all fermions are identical to their SM strength independently of $\tan\beta$ and the mass of the charged Higgs boson.

The SO(5) symmetry of the MS-2HDM is broken explicitly by RG effects due to the $\mathrm{U}(1)_Y$ gauge coupling and equally sizably by the Yukawa couplings of the third generation of quarks and charged leptons. For phenomenological reasons, we have also added a soft SO(5)-breaking bilinear mass parameter m_{12}^2 to the scalar potential, which lifts the masses of all pseudo-Goldstone bosons $h^\pm$, h, and a above the 500 GeV range in agreement with B-meson constraints. To evaluate the RG running of the quartic couplings and the relevant SM couplings, we have employed two-loop 2HDM RGEs from the unification scale μ_X up to charged Higgs-boson mass $M_{h^\pm}$. At the RG scale $M_{h^\pm}$, we have implemented matching conditions between the MS-2HDM and the SM parameters.

Improving upon an earlier study [22], we have now explicitly demonstrated that in the MS-2HDM all quartic couplings can unify at much larger RG scales μ_X, where μ_X lies between $\mu_X^{(1)} \sim 10^{11}$ GeV and $\mu_X^{(2)} \sim 10^{20}$ GeV. In particular, we have shown that quartic coupling unification can take place in two different conformally invariant points, at which all quartic couplings vanish. This property is unique for this model and can happen at different threshold scales $M_{h^\pm} = 500$ GeV, 1 TeV, 10 TeV, and 100 TeV. More precisely, the low-scale (high-scale) unification point arises when λ_2 crosses zero and becomes negative (positive) at the RG scale $\mu_X^{(1)}$ ($\mu_X^{(2)}$). The region between these two scales corresponds to negative values of λ_2. For this reason, we have performed a vacuum stability analysis of the model in order to ensure that the EW vacuum is sufficiently long-lived. In this respect, we have estimated the EW vacuum lifetime τ which was found to be reassuringly long, i.e., much larger than that of the EW vacuum lifetime in the SM, $\tau_{\rm SM} \sim 10^{640} T_U$, assuming the absence of harmful Planck-scale suppressed operators.

It is important to reiterate here that the MS-2HDM is a very predictive extension of the SM, as it is governed by only three additional parameters: (i) the charged Higgs-boson mass $M_{h^\pm}$ (or m_{12}^2), (ii) the ratio of VEVs $\tan\beta$, and (iii) the conformally invariant quartic coupling unification scale μ_X which can take only two discrete values: $\mu_X^{(1)}$ and $\mu_X^{(2)}$. Given these three parameters, the entire Higgs sector of the model can be determined. In this context, we have presented illustrative predictions of misalignment for the SM-like Higgs-boson couplings to the $W^\pm$ and Z bosons and, *for the first time*, to the top and bottom quarks. The predicted deviations to $Hb\bar{b}$ coupling is of order 10% and may be observable to future precision collider experiments.

Evidently, our novel theoretical framework can be straightforwardly extended to multi-HDMs with n scalar-doublets based on the maximal symmetry group $\mathrm{Sp}(2n)/Z_2 \otimes \mathrm{SU}(2)_L$. We plan to report progress on this issue in an upcoming publication.

ACKNOWLEDGMENTS

The work of A. P. and N. D. is supported in part by the Lancaster-Manchester-Sheffield Consortium for Fundamental Physics, under STFC Research Grant No. ST/P000800/1. The work of N. D. is also supported in part by the Polish National Science Centre HARMONIA grant under Contract No. UMO- 2015/18/M/ST2/00518.

[1] S. L. Glashow, Nucl. Phys. **22**, 579 (1961); J. Goldstone, A. Salam, and S. Weinberg, Phys. Rev. **127**, 965 (1962).
[2] S. Weinberg, Phys. Rev. Lett. **19**, 1264 (1967).
[3] A. Salam, *Elementary Particle Physics: Relativistic Groups and Analyticity, Eighth Nobel Symposium* (Almqvist and Wiksell, Stockholm, 1968), p. 367.
[4] F. Englert and R. Brout, Phys. Rev. Lett. **13**, 321 (1964).
[5] P. W. Higgs, Phys. Rev. Lett. **13**, 508 (1964).
[6] ATLAS Collaboration, Phys. Lett. B **716**, 1 (2012).
[7] CMS Collaboration, Phys. Lett. B **716**, 30 (2012).
[8] ATLAS Collaboration, CERN Report No. ATLAS-CONF-2019-004, 2019.
[9] CMS Collaboration, CERN Report No. CMS-PAS-SMP-19-001, 2019.
[10] T. D. Lee, Phys. Rev. D **8**, 1226 (1973).
[11] G. C. Branco, P. M. Ferreira, L. Lavoura, M. N. Rebelo, M. Sher, and J. P. Silva, Phys. Rep. **516**, 1 (2012).
[12] A. Arbey, F. Mahmoudi, O. Stal, and T. Stefaniak, Eur. Phys. J. C **78**, 182 (2018).
[13] E. Hanson, W. Klemm, R. Naranjo, Y. Peters, and A. Pilaftsis, arXiv:1812.04713.
[14] S. L. Glashow and S. Weinberg, Phys. Rev. D **15**, 1958 (1977).
[15] L. J. Hall and M. B. Wise, Nucl. Phys. **B187**, 397 (1981).
[16] V. D. Barger, J. L. Hewett, and R. J. N. Phillips, Phys. Rev. D **41**, 3421 (1990).
[17] A. Pich and P. Tuzon, Phys. Rev. D **80**, 091702 (2009).
[18] I. F. Ginzburg, M. Krawczyk, and P. Osland, arXiv:hep-ph/9909455.
[19] P. H. Chankowski, T. Farris, B. Grzadkowski, J. F. Gunion, J. Kalinowski, and M. Krawczyk, Phys. Lett. B **496**, 195 (2000).
[20] A. Delgado, G. Nardini, and M. Quiros, J. High Energy Phys. 07 (2013) 054.
[21] M. Carena, I. Low, N. R. Shah, and C. E. M. Wagner, J. High Energy Phys. 04 (2014) 015.
[22] P. S. B. Dev and A. Pilaftsis, J. High Energy Phys. 12 (2014) 024; 11 (2015) 147(E).
[23] J. Bernon, J. F. Gunion, H. E. Haber, Y. Jiang, and S. Kraml, Phys. Rev. D **92**, 075004 (2015).
[24] K. Benakli, M. D. Goodsell, and S. L. Williamson, Eur. Phys. J. C **78**, 658 (2018).
[25] K. Lane and W. Shepherd, Phys. Rev. D **99**, 055015 (2019).
[26] B. Grinstein and P. Uttayarat, J. High Energy Phys. 06 (2013) 094; 09 (2013) 110(E).
[27] J. Baglio, O. Eberhardt, U. Nierste, and M. Wiebusch, Phys. Rev. D **90**, 015008 (2014).
[28] N. Darvishi and M. Krawczyk, Nucl. Phys. **B926**, 167 (2018).
[29] A. Pilaftsis, Phys. Lett. B **706**, 465 (2012).
[30] A. Pilaftsis, Phys. Rev. D **93**, 075012 (2016).
[31] P. S. B. Dev and A. Pilaftsis, J. Phys. Conf. Ser. **873**, 012008 (2017).
[32] H. Georgi and D. V. Nanopoulos, Phys. Lett. **82B**, 95 (1979).
[33] J. F. Gunion and H. E. Haber, Phys. Rev. D **67**, 075019 (2003).
[34] I. F. Ginzburg and M. Krawczyk, Phys. Rev. D **72**, 115013 (2005).
[35] H. E. Haber and O. Stål, Eur. Phys. J. C **75**, 491 (2015); **76**, 312(E) (2016).
[36] B. Grzadkowski, H. E. Haber, O. M. Ogreid, and P. Osland, J. High Energy Phys. 12 (2018) 056.
[37] V. Branchina and E. Messina, Phys. Rev. Lett. **111**, 241801 (2013).
[38] V. Branchina, F. Contino, and A. Pilaftsis, Phys. Rev. D **98**, 075001 (2018).
[39] J. Goldstone, Nuovo Cimento **19**, 154 (1961).
[40] P. Minkowski, Phys. Lett. **67B**, 421 (1977); T. Yanagida, Prog. Theor. Phys. **64**, 1103 (1980); R. N. Mohapatra and G. Senjanovic, Phys. Rev. Lett. **44**, 912 (1980); J. Schechter and J. W. F. Valle, Phys. Rev. D **22**, 2227 (1980).
[41] R. A. Battye, G. D. Brawn, and A. Pilaftsis, J. High Energy Phys. 08 (2011) 020.
[42] C. C. Nishi, Phys. Rev. D **83**, 095005 (2011).
[43] I. P. Ivanov, Phys. Rev. D **77**, 015017 (2008).
[44] P. M. Ferreira, H. E. Haber, and J. P. Silva, Phys. Rev. D **79**, 116004 (2009).
[45] P. M. Ferreira, H. E. Haber, M. Maniatis, O. Nachtmann, and J. P. Silva, Int. J. Mod. Phys. A **26**, 769 (2011).
[46] K. A. Olive *et al.* (Particle Data Group), Chin. Phys. C **38**, 090001 (2014).
[47] R. D. Peccei and H. R. Quinn, Phys. Rev. Lett. **38**, 1440 (1977).
[48] S. Weinberg, Phys. Rev. Lett. **40**, 223 (1978).
[49] F. Wilczek, Phys. Rev. Lett. **40**, 279 (1978).
[50] M. Misiak and M. Steinhauser, Eur. Phys. J. C **77**, 201 (2017).
[51] J. Oredsson and J. Rathsman, J. High Energy Phys. 02 (2019) 152.
[52] D. Chowdhury and O. Eberhardt, J. High Energy Phys. 11 (2015) 052.
[53] M. E. Krauss, T. Opferkuch, and F. Staub, Eur. Phys. J. C **78**, 1020 (2018).
[54] A. V. Bednyakov, J. High Energy Phys. 11 (2018) 154.
[55] F. Staub, Comput. Phys. Commun. **185**, 1773 (2014).
[56] M. Carena, J. Ellis, J. S. Lee, A. Pilaftsis, and C. E. M. Wagner, J. High Energy Phys. 02 (2016) 123.
[57] D. Buttazzo, G. Degrassi, P. P. Giardino, G. F. Giudice, F. Sala, A. Salvio, and A. Strumia, J. High Energy Phys. 12 (2013) 089.
[58] N. G. Deshpande and E. Ma, Phys. Rev. D **18**, 2574 (1978).
[59] G. Aad *et al.* (ATLAS and CMS Collaborations), J. High Energy Phys. 08 (2016) 045.
[60] G. C. Branco, Phys. Rev. D **22**, 2901 (1980).
[61] M. Sher, Phys. Rep. **179**, 273 (1989).
[62] P. M. Ferreira, R. Santos, and A. Barroso, Phys. Lett. B **603**, 219 (2004); **629**, 114(E) (2005).
[63] I. P. Ivanov, Phys. Rev. D **75**, 035001 (2007); **76**, 039902(E) (2007).
[64] V. Branchina, F. Contino, and P. M. Ferreira, J. High Energy Phys. 11 (2018) 107.
[65] S. R. Coleman, Phys. Rev. D **15**, 2929 (1977); **16**, 1248(E) (1977).
[66] P. B. Arnold and S. Vokos, Phys. Rev. D **44**, 3620 (1991).
[67] S. Fubini, Nuovo Cimento A **34**, 521 (1976).